Time-resolved imaging of gas phase nanoparticle synthesis by laser ablation

David B. Geohegan, Alex A. Puretzky, Gerd Duscher, and Stephen J. Pennycook
Solid State Division, Oak Ridge National Laboratory, Oak Ridge, Tennessee 37831-6056

(Received 20 February 1998; accepted for publication 2 April 1998)

The dynamics of nanoparticle formation, transport, and deposition by pulsed laser ablation of *c*-Si into 1–10 Torr He and Ar gases are revealed by imaging laser-induced photoluminescence and Rayleigh-scattered light from gas-suspended 1–10 nm SiO_x particles. Two sets of dynamic phenomena are presented for times up to 15 s after KrF-laser ablation. Ablation of Si into heavier Ar results in a uniform, stationary plume of nanoparticles, while Si ablation into lighter He results in a turbulent ring of particles which propagates forward at 10 m/s. Nanoparticles unambiguously formed in the gas phase were collected on transmission electron microscope grids for *Z*-contrast imaging and electron energy loss spectroscopy analysis. The effects of gas flow on nanoparticle formation, photoluminescence, and collection are described. © *1998 American Institute of Physics.* [S0003-6951(98)00223-X]

Thin films containing photoluminescent nanocrystalline Si (*nc*-Si) and silicon-rich silicon oxide (SRSO) nanoparticles have recently been synthesized by laser ablation of Si into 0.2–10 Torr background gases.[1–5] These films are among the most promising optoelectronic materials for applications requiring room-temperature photoluminescence (PL) and compatibility with existing silicon processing technology. Recently, electroluminescent light-emitting diodes were fabricated from laser ablation-produced *nc*-Si films.[6]

Optimizing the synthesis of quantum-confined nanomaterials by laser ablation in background gases requires a knowledge of the temporal and spatial scales for nanoparticle formation, and how nanoparticles are transported and deposited. There is no adequate theoretical description of this process, and experimentally, it is often unclear whether nanoparticles collected on substrates were formed in the gas phase or from nuclei formed on the substrate surface.[3–5]

Several *in situ* measurements of gas-formed nanoparticles have recently been employed using different techniques. In 1994, Chiu *et al.* attempted the first PL measurements of gas-suspended silicon nanocrystals.[5] The nanocrystals were generated in a laser vaporization (Smalley) cluster source, and despite strong Rayleigh scattering (RS) from the particles no detectable PL signal could be observed. Movtchan *et al.* found small (<2 nm) SiO_x clusters in films deposited through low pressure (<1 Torr) gases and reported cluster luminescence (without external excitation) close to the target surface ($d<2$ cm) within delays of $\Delta t<10$ μs after laser ablation. Recently, Muramoto *et al.* used a combination of laser-induced fluorescence imaging from atomic Si and RS from nanoparticles to infer a much later time ($\Delta t>100-200$ μs) for the onset of dimerization and subsequent nanoparticle growth following Si ablation into 10 Torr He.[7]

Here we report the first time-resolved measurements of photoluminescence from gas-suspended nanoparticles and utilize gated ICCD (intensified CCD-array) imaging of this PL (as well as RS) to reveal dramatically different Si-nanoparticle formation and propagation dynamics in He and Ar. Gas-formed nanoparticles are unambiguously collected and analyzed by transmission electron microscopy (TEM).

The experimental apparatus for ICCD photography and spectroscopy of laser ablation plasmas has been described previously.[8–10] Polished *c*-Si wafers were ablated by KrF-laser pulses ($\lambda=248$ nm, focused to energy densities of $5-8$ J/cm^2 in 28 ns pulses, spaced one pulse per minute) inside a large, turbopumped vacuum chamber (1×10^{-6} Torr base pressure) maintained at 1–10 Torr of 99.9999% He or 99.9995% Ar with variable flow controllers (0–1000 sccm).

Figure 1(A) shows a sequence of ICCD photographs detailing the visible plasma luminescence resulting from KrF-laser ablation of silicon into flowing argon gas at 1 Torr. Within $\Delta t=20$ μs, collisions with the background gas rapidly decelerate the plume of silicon vapor from an initial velocity of 2 cm/μs (kinetic energy/atom=58 eV) to only 0.01 cm/μs (0.0015 eV). A backward-propagating flux of material is observed to reflect from the target surface at $\Delta t=300$ μs after ablation, before a relatively uniform cloud of confined plasma forms and cools over several milliseconds.

For RS and PL from clusters suspended in the gas phase, a pulse of light from a XeCl-laser illuminated a slice of the silicon plume from below. Probe laser light scattered by nanoparticles (with estimated diameters larger than 1 nm)[11] was imaged by gating the camera on during the XeCl laser pulse. Alternatively, the camera was gated on after the probe laser pulse to capture images of long-lived photoluminescence.

The first detectable PL (and RS) are observed in Fig. 1(B) at $\Delta t=3$ ms after ablation, just as the last remnants of plasma luminescence disappear [compare with Fig. 1(A)]. The PL images of Fig. 1(B) (also RS images, not shown) indicate that silicon nanoparticles form first near the target surface and then occupy the entire plume volume within the next two milliseconds. Over the next hundreds of milliseconds, the stationary nanoparticle cloud densifies near the center of the initial ($\Delta t=5$ ms) spatial distribution. We believe that outward diffusion of atoms or small clusters on the outer edges of the cloud does not lead to aggregation into larger nanoparticles, while inward diffusion does. This cloud of nanoparticles is eventually blown upward in Fig. 1(C) by

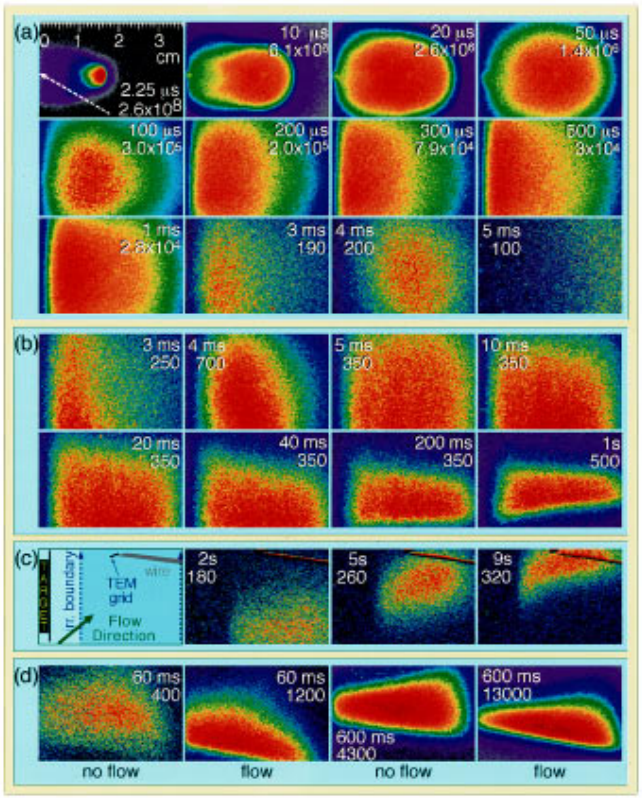

FIG. 1. (A) Gated-ICCD photographs of the nascent visible plasma luminescence observed when a 2″ *c*-Si wafer (left of frame) is laser-ablated (KrF, 28 ns FWHM pulse, incident at 30° as shown) into 1 Torr Ar (5 ns to 15 μs exposures). The time delay after ablation and the maximum intensity (red) of each image are listed. (B) 3 μs exposures of PL from nanoparticles after a XeCl-laser pulse (308 nm, 4.0 eV, 30 ns FWHM, $\sim$0.2 J/cm^2 in 3.5 cm$\times$0.15 cm beam) is directed vertically through the plume at the indicated times after laser ablation. (C) PL images of the nanoparticle cloud swept by the weak argon flow onto a TEM grid for subsequent analysis. (D) Rayleigh-scattered light from nanoparticles is imaged at two times (60 and 600 ms) after laser ablation into static (''no-flow'') or flowing (''flow'', 270 sccm) 1 Torr Ar.

the weak flow in the chamber (270 sccm into 50 *l* chamber) onto a TEM grid suspended by a thin wire.

Remarkably, no PL is observed when silicon is ablated into nonflowing argon. However RS images revealed that nonluminescing nanoparticles were present in nearly equal numbers. Figure 1(D) compares RS images under flow and no-flow conditions at $\Delta t = 60$ and 600 ms. The weak Ar flow [see Fig. 1(C)] also significantly alters the particle growth, as indicated by the RS intensity in Fig. 1(D) ($\propto d^6 N$, where d, N are the particle diameter, density).[11]

Copper and holey carbon TEM grids were positioned on wire armatures in the chamber to collect the luminescing species. PL and RS photography permitted direct imaging and control of the deposition process [as in Figs. 1(C) and 3(A)]. The grids were exposed to room air for less than 2 min during loading into a VG HB501UX scanning transmission electron microscope for *Z*-Contrast imaging.

For the particles shown in Figs. 2(B) and 2(C), the grid was held 10 cm above the imaged cloud until $\Delta t = 1.0$ s, and then swept through the cloud at $d = 2$ cm from $\Delta t = 1.0 - 1.5$ s. This was repeated for 10 ablation events. Isolated, spherical, 4–5 nm diameter nanoparticles were typically found with other sizes ranging from 1 to 10 nm. Depending on the distance and flow conditions, a range of SiO_x

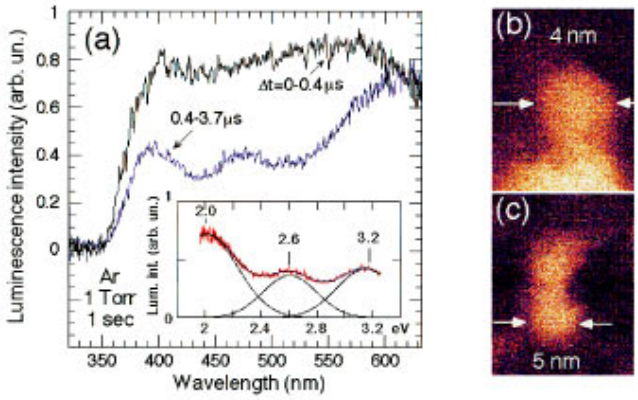

FIG. 2. (A) Photoluminescence spectra of gas-suspended nanoparticles located $d = 2$ cm from a *c*-Si target in 1 Torr flowing Ar at $\Delta t = 1$ s after KrF-laser ablation. Luminescence was acquired at two time delays following the initiation of the 30 ns FWHM XeCl-laser excitation pulse: 0–0.4 and 0.4–3.7 μs. The inset shows the 0.4–3.7 μs spectrum in energy units, deconvoluted into bands at 2.0, 2.6, and 3.1 eV. (B), (C) *Z*-Contrast TEM images of nanoparticles collected at $\Delta t = 1 - 1.5$ s, $d = 2$ cm in 1 Torr Ar.

stoichiometries ($0 < x < 2$) were obtained. Detailed PL spectra of gas-suspended nanoparticles, deposited films, and correlated particle analysis will be presented in a separate letter.[12]

PL spectra of gas-phase nanoparticles were recorded with a gated-intensified diode array (Princeton Inst.) on a 0.3 m monochromator (Acton VM-503, 150 grooves/mm grating, 10 nm resolution). In this case, the sheet of XeCl light was turned parallel to the target surface.

A representative PL spectrum is given in Fig. 2(A) for Si ablation into flowing 1 Torr Ar acquired at $d = 2$ cm and at $\Delta t = 1.0$ s [see Fig. 1(B), 1.0 s]. Three broad photoluminescence bands were found for both argon and helium. These bands agree with those observed for oxidized *nc*-Si films and porous silicon.[13,14] The violet (3.2 eV) band emerged to dominate at later time delays for both He and Ar and correlated with the extent of oxidation as determined by *ex situ* TEM analysis.[12] Measured luminescence decay times ranged up to 2 μs [see Fig. 2(A)].

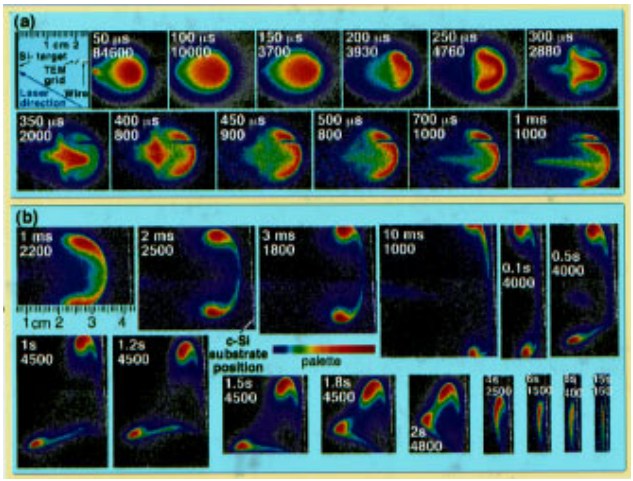

FIG. 3. (A) ICCD images of plasma luminescence ($\Delta t < 400$ μs) plus photoluminescence ($\Delta t > 200$ μs) from nanoparticles produced by silicon ablation into 10 Torr He (3 μs exposures). (B) PL images at later times show the swirling smoke-ring of nanoparticles encountering a room-temperature silicon wafer (at the dashed line position).

For Fig. 1(B), the flow of argon was varied from 1 to 1000 sccm and optimized (at 270 sccm) to maximize the integrated PL intensity. The formation of photoluminescent SRSO stoichiometries appears to depend upon the rates for silicon-silicon clustering and silicon oxidation during nanoparticle growth. Small admixtures of oxygen in the gas flow quenched the violet PL, as did stopping the flow.

Although small silicon clusters have been measured to be about two orders of magnitude less reactive than a bare silicon surface,[15,16] the environment in the ablation plume appears to be considerably more reactive. Oxygen was present in only 1–5 ppm levels from H_2O and O_2 impurities in the high purity rare gases, from the chamber walls, and from the reoxidized target surface. Gas flow was essential to bring fresh oxygen-containing molecules into the vicinity of the stationary Si/Ar plume to achieve photoluminescent SRSO stoichiometries.

A strikingly different set of dynamics are initiated by ablation of Si into 10 Torr He, presented in Fig. 3. In Fig. 3(A), the laser-induced PL is imaged along with the plasma luminescence (which rapidly drops during the first 400 μs after ablation). By comparing images with and without the excitation pulse, the laser-induced PL (and RS, not shown) could be first discerned at $\Delta t = 150-200$ μs, near the front of the expanding plume. From $\Delta t = 200-400$ μs, the intensity of RS and PL increases at the front of the plume, while a central core of clusters (too small to scatter light) suddenly appears as the brightest region in the images at $\Delta t = 250$ μs, and then collapses to the center of the plume, following the extinguishing core of plasma luminescence. These measured times for the onset of clustering agree with LIF measurements of Muramoto *et al.*[7]

The surviving nanoparticles at $\Delta t = 500$ μs form a shell of material. As shown in Fig. 3(B), the nanoparticles segregate over the next two milliseconds into a swirling ''smoke ring'' which grows in diameter as it propagates forward at 10 m/s. A weak central trail of nanoparticles is also visible.

In Fig. 3(B), the moving nanoparticles encounter a room-temperature silicon wafer under typical deposition conditions. The presence of the substrate halts the nanoparticles after a few milliseconds but they do not readily deposit, and remain nearly motionless for several seconds. Aggregation appears to occur during this period since the volume of the nanoparticle region again decreases, while the PL and RS intensities increase. After several seconds, the separated balls of nanoparticles may come near one another [as shown in Fig. 3(B) for $\Delta t = 0.5-2.0$ s] due to flow conditions in the chamber. At these times, the two balls are apparently attracted to each other by the pressure drop induced by agglomeration. The entire 15 s dynamic sequence of Fig. 3 was remarkably reproducible.

Photoluminescent nanoparticles were formed in 10 Torr helium regardless of the flow conditions. Unlike the propagation in static argon, the turbulent mixing and forward propagation of the plume in helium introduced fresh oxygen-containing molecules to the condensing nanoparticles.

The mass ratio between plume (Si) and background gas atoms (Ar, He) has been shown to have a major effect on the plume dynamics in the 0–1 Torr pressure range.[17] Experiments[9,10] and multiple-scattering simulations show that heavier Ar atoms ($m = 40$) effectively remove Si atoms ($m = 28$) from the forward-going flux, and can even scatter Si atoms backward, while lighter He atoms ($m = 4$) gradually slow Si atoms with a series of small-angle collisions.[17]

In summary, the nanoparticle synthesis and transport dynamics reported here were considerably different for argon and helium. Argon (1.0 Torr) stops and reflects the Si plume, resulting in a stationary, uniformly distributed nanoparticle cloud. Helium (10 Torr) slows the silicon plume, angularly segregating most of the nanoparticles to a turbulent smoke ring which propagates at ~ 10 m/s through the chamber. Onset times for nanoparticle formation (3 ms in 1 Torr Ar, 0.15–0.2 ms in 10 Torr He) were measured by both PL and RS. In both cases, nanoparticles appeared as the plasma luminescence extinguished.

Time-resolved photoluminescence from gas-suspended nanoparticles was measured for the first time. Three broad bands of photoluminescence (2.0, 2.6, and 3.2 eV) similar to those of oxidized *nc*-Si were measured and correlated with 1–10 nm diameter, spherical SiO_x particles collected from the gas phase.

Coupled with RS, *in situ* PL imaging and spectroscopy provide a new approach to study and control the photoluminescence properties of isolated nanoparticles, prior to deposition. The observed dynamics suggest new ways to optimize the production, doping, and collection of gas-constructed nanomaterials by laser ablation.

The authors gratefully acknowledge research assistance by C. W. White and B. C. Sales and valuable discussions with T. Okada, W. Marine, T. Makimura, K. Murakami, Y. Yamada, T. Yoshida, R. F. Wood, J.-N. Leboeuf, D. H. Lowndes, and K. P. Geohegan. This work was sponsored by the Division of Material Science, U. S. Department of Energy under Contract No. DE-AC05-96-R22464 with Lockheed Martin Energy Research Corp.

[1] Y. Yamada, T. Orii, I. Umezu, S. Takeyama and T. Yoshida, Jpn. J. Appl. Phys., Part 1 **35**, 1361 (1996).
[2] T. Makimura, Y. Kunii, and K. Murakami, Jpn. J. Appl. Phys., Part 1 **35**, 4780 (1996).
[3] S. Li, S. J. Silvers, and M. S. El-Shall, J. Phys. Chem. B **101**, 1794 (1997).
[4] I. A. Movtchan, W. Marine, R. W. Dreyfus, H. C. Le, M. Sentis, and M. Autric, Appl. Surf. Sci. **96-98**, 251 (1996).
[5] L. A. Chiu, A. A. Seraphin, and K. D. Kolenbrander, J. Electron. Mater. **23**, 347 (1994).
[6] T. Yoshida, Y. Yamada, and T. Orii, Technical Digest of the International Electron Devices Meeting, IEEE, San Francisco, CA, Dec. 8–11, 1996.
[7] J. Muramoto, Y. Nakata, T. Okada, and M. Maeda, Jpn. J. Appl. Phys., Part 2 **36**, L563 (1997).
[8] D. B. Geohegan, Appl. Phys. Lett. **60**, 2732 (1992).
[9] D. B. Geohegan and A. A. Puretzky, Appl. Phys. Lett. **67**, 197 (1995).
[10] D. B. Geohegan and A. A. Puretzky, Appl. Surf. Sci. **96-98**, 131 (1996).
[11] H. C. van de Hulst, Light Scattering by Small Particles (Dover, New York, 1981).
[12] D. B. Geohegan, A. A. Puretzky, G. Duscher, and S. J. Pennycook (unpublished).
[13] P. M. Fauchet, J. Lumin. **70**, 294 (1996).
[14] F. Koch and V. Petrova-Koch, J. Non-Cryst. Solids **198-200**, 846 (1996).
[15] M. F. Jarrold, Science **252**, 1085 (1991).
[16] E. C. Honea, J. S. Kraus, J. E. Bower, and M. F. Jarrold, Z. Phys. D **26**, 141 (1993).
[17] R. F. Wood, K. R. Chen, J. N. Leboeuf, A. A. Puretzky, and D. B. Geohegan, Phys. Rev. Lett. **79**, 1571 (1997).